Journal of Materials Chemistry A

Accepted Manuscript

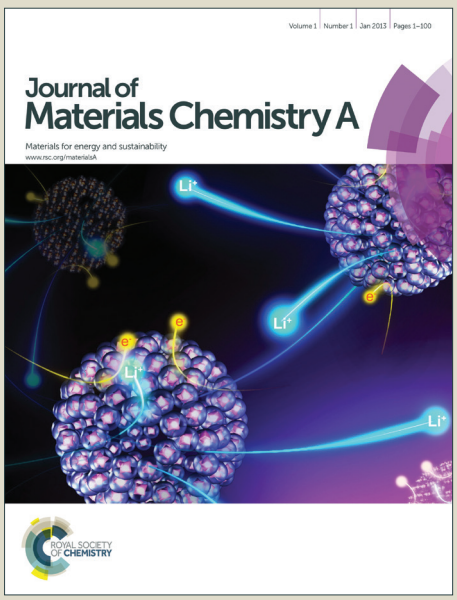

ROYAL SOCIETY OF CHEMISTRY

www.rsc.org/materialsA

Harvesting broadband absorption of solar spectrum for enhanced photocatalytic H_2 generation

Peh Kang Nuo Connor, Minmin Gao and Ghim Wei Ho[a,b,c,*]

[a] *Engineering Science Programme, National University of Singapore, 4 Engineering Drive 3, 117576, Singapore*

[b] *Department of Electrical and Computer Engineering, National University of Singapore, 4 Engineering Drive 3, 117576, Singapore*

[c] *Institute of Materials Research and Engineering, A*STAR (Agency for Science, Technology and Research), 3 Research Link, 117602, Singapore.*

*Corresponding author: Dr. Ghim Wei Ho Email: elehgw@nus.edu.sg

Abstract

Absorption of the solar spectrum in the visible and near infrared region is highly desirable to improve photocatalytic H_2 generation. Traditionally, this can be fulfilled by designing photocatalyst materials with narrower band gaps, or with upconversion capabilities. However such materials often pose challenges such as in synthesis, structural defects, stability which may lead to adverse photocatalytic performance. This paper focuses on broadband utilization of solar spectrum for enhanced photocatalysis solar H_2 production where the spectrum not utilized by the photocatalysts is absorbed and converted to heat energy. This approach delves into harvesting broadband spectrum for synergistic photocatalysis and thermal heat generation, with minimal photocatalyst materials manipulation. The profound impact of temperature on photocatalysis was manifested in a drastic increase of H_2 production by a maximum of 40-fold. Apparent quantum yield was also calculated to reach 66.9% using an ultraviolet LED light source. Outdoor testing verifies the potential of broad spectrum operation under natural sunlight as well as the convenience and simplicity of various reactor designs for practical photocatalysis applications.

Keywords

Solar hydrogen production; Broadband solar absorption; Solar heating; CuO-TiO_2 composite; Photocatalyst

INTRODUCTION

TiO_2 is a widely studied material in photocatalytic water splitting due to its abundance, environmentally-friendliness, and stability.[1-3] However, TiO_2 only generates H_2 in pure water at a low rate due to the fast recombination of electron-hole pairs, and has a fast backward reaction, in addition to the ability to absorb only the UV spectrum.[4] Co-catalyst loading such as Pt deposition on TiO_2 has been proven to increase H_2 production under solar water splitting by preventing the recombination of electron-hole pairs.[5-7] However, Pt and other various rare and expensive noble metal co-catalysts (like Au and Pd) limit the scale of implementation for extensive water splitting, thus other cost-effective co-catalysts have been explored. Copper oxide as a co-catalyst has been studied by several groups have shown to improve H_2 production rate by ~30 to 129 fold compared to pure TiO_2[8-13], achieving a rate of 5.133mmol/gh using a Hg lamp in 5% vol methanol in water,[9] and 2.061mmol/gh in 0.1M of aqueous glycerol with an apparent quantum yield (AQY) of 13.4% using a 365 nm LED.[11] Other earth abundant co-catalysts such as Ni were also explored. Ni-loaded TiO_2 produced H_2 at a rate of 2.547 mmol/gh with an AQY of 8.1% using a 365 nm UV LED.[14] In comparison, an AQY of 70% was measured for Pt-loaded TiO_2 photocatalyst using a black lamp (365 nm) in 1M of aqueous glycerol,[15] while a graphene based Au-loaded TiO_2 photocatalyst produced 0.296 mmol/gh of H_2, with a AQY of 4.1% using a 420 nm LED in ethanol (25 % vol)-water.[16] Using earth abundant co-catalysts allows for economical and effective catalyst material development for solar water splitting, with performance that can be compared to noble metal co-catalyst loading.

To better utilize solar energy, research has been focused on developing semiconductor photocatalysts that can harvest a wider spectrum of solar radiation to increase the absorption of useful photons for conversion to H_2. However, most are focused on development of visible-light-induced photocatalysts, with visible light irradiation (400-750nm) accounting for 43% of the incoming solar energy. For the case of TiO_2, doping with metal cations and/or anions to decrease the band gap is often carried out.[4, 5, 17-22] However, doping often leads to poorer performances as defects and traps are introduced, causing unwanted recombination of the photogenerated electron-hole pairs. For example, black TiO_2 has been synthesized by hydrogenation of TiO_2 nanoparticles under high temperature and pressure. This created disorder in the TiO_2 nanoparticles and causing a narrower band gap and extending the absorption into the visible-near infrared range. A H_2 production rate of 10 mmol/gh was achieved under a solar simulator in 50% vol methanol in water.[23] Narrow band gap

semiconductors like metal oxynitrides, nitrides, sulphides or phosphides have also been explored as an effort to harness more of the solar spectrum, but they tend to be unstable, undergoing photocorrosion in the presence of visible light. These materials oxidize during the water splitting process, and thus degrade over time.[24-26] Pt_3Co-loaded CdS was shown to have a H_2 production rate of 15.89 mmol/gh using a Xe lamp with a 420 nm cutoff filter, with a 10% vol aqueous lactic acid solution.[27] ZnS-based solid solutions are efficient and low-toxic visible-light driven photocatalyst, and Yu *et al.* has synthesized Cu^{2+}-modified a $Zn_xCd_{1-x}S$ with a high H_2 production rate of 4.639 mmol/gh, and an AQY of 20.9% at the visible wavelength of 420 nm, in a solution of Na_2S/Na_2SO_3 sacrificial reagent to suppress photocorrosion.[28] Wang *et al.* has also synthesized ZnO@ZnS–Bi_2S_3 core–shell nanorods anchored on reduced graphene oxide, with a H_2 production rate of 0.310 mmol/gh in a solution of 5% glycerol under a 1000W/m^2 Xe lamp illumination. [29]

Even if the UV to visible light can be fully harvested, the utilization of solar energy is still limited to 51%. Most importantly, harvesting of full visible light radiation by a photocatalyst material is not achievable since the near infra-red (750-2500 nm) region, which accounts for 38.6% of solar energy remains unutilized due water splitting nature which requires photocatalysts to have a minimum band gap of 1.5 -2.0 eV, taking the overpotentials into account.[30] Subsequently, the photocatalyst search is extended to near-infrared light photocatalysts which limit mainly to upconversion luminescence of rare earth materials.[31, 32] Upon near-infrared excitation, the rare earth material generates upconverted emission peaks ranging from near-infrared to UV. Though the upconversion crystal exploits the near infrared solar spectrum, the absorption profile consists of discrete wavelengths, rather than a band of wavelengths. Furthermore, the upconversion intensity is low and often requires a laser to excite.

It can be seen that utilization of the broadband solar spectrum for photocatalysis remains a significant challenge, especially in the near infrared region which has insufficient energy to carry out the photogeneration of H_2 from water splitting. Utilizing the visible and near infrared portion of the solar spectrum to enhance solar H_2 production with minimal effort and nominal materials manipulation is the focus of this work. Specifically, the unabsorbed solar spectrum is used for heat generation to increase the temperature of the photocatalysis system, which has explicitly shown to prolong the lifetime of the photogenerated carriers and hence drastically improve the rate of H_2 production. To date, we have not seen any studies that specifically exploit sunlight for this purpose of heat generation to synergistically improve

photocatalytic hydrogen production. Thus, simple prototypes were constructed to demonstrate the proof-of-concept harvesting of broadband solar energy for photon and heat conversions to enable practical and efficient solar-energy conversion photocatalysis.

RESULTS AND DISCUSSION

The SEM images in Figure 1(a) and inset depict TiO_2 nanotubes with a uniform cylindrical structure of length ~200 nm and diameter ~10 nm. The TEM images in Figure 1(b) show that TiO_2 nanotubes structure can be seen clearly with the darker edges and the lighter contrast in the center of the tube. Well-dispersed and uniform CuO nanoparticles are seen loaded onto the surface of the TiO_2 nanotubes, having a diameter of a few nanometers. The Figure 1(b) inset shows the high resolution TEM diffraction fringe pattern of one of the CuO nanoparticles, with a lattice spacing of 2.31Å corresponding to the (111) plane of CuO. Figure 1(c) shows the XRD patterns of the TiO_2 nanotubes as well as for TiO_2 nanoparticles, after $Cu(NO_3)_2$ addition. The XRD peaks for nanoparticles correspond to both TiO_2 anatase and rutile phases, while the TiO_2 nanotubes contain only the TiO_2 anatase phase. The presence of CuO diffraction peaks indicates the formation of CuO-TiO_2 composite.

UV-vis spectra are shown for nanoparticles and nanotubes samples with and without CuO loading (Figure 1 (d)). They are measured before and after a period of 10 min UV illumination. It is observed that nanoparticles show absorption edge at around 400 nm, while the nanotubes absorption edges are seen around 380 nm. This is attributed to nanotubes having a pure anatase TiO_2 phase of band gap 3.2-3.3eV, compared to the nanoparticles which is a mixture of rutile (smaller bandgap) and anatase phase. In general, there is a slight increase in absorption after UV illumination for all samples. This corresponds to the samples turning slightly grey due to the oxygen vacancies[33-36] which reverted back to white colour on contact with air/oxygen. The CuO-loaded samples turned purplish-grey upon UV illumination which corresponded to a local maximum in the absorption spectra at ~ 580 nm, as well as an increase in absorption across the wavelength range. The presence of the specific absorption peak and the change in color are postulated to the reduction of the CuO by the transfer of electron from the TiO_2 conduction band to the adsorbed CuO nanoparticles (Figure S1). [9, 12, 37, 38]

Brunauer–Emmett–Teller (BET) specific surface area and pore distribution were determined using nitrogen isothermal adsorption and desorption. The nitrogen adsorption/desorption curve (Figure 1 (e), S2) displayed H3 hysteresis loops, suggesting the presence of mesopores.

With calculations based on desorption branches using the BET and Barrett–Joyner–Halenda model, the determined specific surface area of nanoparticles are 48.7 m^2/g and 51.8 m^2/g, while the specific area of NT are 154.4 m^2/g and 110.7 m^2/g before and after CuO loading, respectively. The pore radius is measured to be ~ 13-14 nm for nanoparticles and ~ 9 nm for the nanotubes samples regardless of CuO loading. The higher specific areas of nanotubes imply more active surface sites for the photogeneration to take place, beneficial for the phototcatalysis.

In order to optimize the photocatalytic H_2 production, CuO loading of different weight percentages (0-5 wt%) onto TiO_2 nanoparticles (using commercial P25 as a standard reference) and nanotubes were carried out (Figure 2(a),(b)). It can be observed that the CuO loading has substantial effect on the photocatalytic properties, as such even the lowest CuO loading of 1% show significant improvement in H_2 generation performance by around 37 and 40-fold for nanoparticles and nanotubes samples, respectively. Notably, the improvement in H_2 production is higher for nanotubes possibly due to their higher specific surface as determined from the BET. It is also noted that 3 % CuO loading have consistently showed the best photocatalytic performance for both nanoparticles and nanotubes. Photocatalytic H_2 production enhancement of ~ 54-fold has been attained for both samples, with a rate of 4.10 mmol/gh and 5.40 mmol/gh for CuO-loaded nanoparticles and nanotubes respectively. This is comparable to other studies done on CuO-TiO_2.[9-12, 39]

It is postulated that the loaded CuO nanoparticles will reduce to Cu_2O or Cu nanoparticles by accepting photogenerated electrons generated by UV light irradiation in TiO_2.[10] The reduced CuO nanoparticles co-catalyst introduce active sites for H_2 evolution such that electrons generated in TiO_2 can be easily transferred to the co-catalyst, thus function as effective trapping centers.[35] Hence the co-catalyst nanoparticles loaded on TiO_2 photocatalyst is well-suited for charge separation as after the electron-hole pair generation, the electron is transferred into the conduction band of the co-catalyst, which is below that of the photocatalyst, effectively inhibited recombination.[9, 11-13, 37, 38] However, higher loading of CuO nanoparticles > 3 % is seen to decrease the rate of H_2 generation, possibly due to excessive loading which leads to particle agglomeration, consequently shield the photosensitive TiO_2 surfaces. It is also suggested that overloading of CuO co-catalyst may absorb the photons, hence reducing the photoexcitation capacity of TiO_2.[38]

We also examined the heat absorbing effect of CuO-loading under full spectrum illumination. NT and CuO-NT photocatalysts were each placed in 10 ml of (20% vol) glycerol solution in a 25 ml quartz reactor, and was placed under a Xe lamp illumination at 1000W/m^2, equivalent to 1 sun's intensity. The photocatalysts would absorb heat from the direct illumination of the Xe lamp and cause the temperature to rise. The reactors were first placed in an ice water bath to ensure the initial temperatures were the same. We observed that after the CuO-NT photocatalysts had a faster increase in temperature, as well as a higher final temperature after 30 mins (Figure S3). This can be associated to the darker color of the photocatalysts from the CuO nanoparticles as evidenced by the UV-Vis spectrum, which allowed for a greater absorbance of the incoming light and converted a portion of it to low-grade heat.

Photocatalytic H_2 production under UV illumination was also done at various temperatures with glycerol as the sacrificial reagent, to study the effect of temperature on photocatalysis. Glycerol was chosen as the sacrificial agent in this case as the boiling point of a water-glycerol solution is above 100 °C, which is higher than a methanol-water mixture (methanol boiling point ~ 64.7 °C). Furthermore, glycerol is a byproduct of biodiesel available in large quantities and treated as a waste material.[40-42] It is observed that increasing the photocatalysis temperature from 25 to 90 °C boosted the rate of H_2 production of the pure TiO_2 nanoparticles and nanotubes up to 20 and 40-fold, respectively (Figure 2 (c), (d), Table S1). The CuO loaded TiO_2 samples also showed an improvement in the H_2 production of 5 and 7-fold corresponding to the nanoparticles and nanotubes samples. On the whole, a remarkable improvement in photocatalytic H_2 production of ~300 to 350-fold are observed for the pristine TiO_2 samples after co-catalyst loading and operation at elevated photocatalysis temperature.

Some possible reaction pathways for the photocatalytic production of H_2 from glycerol have been studied and proposed in literature. Panagiotopoulou et al. has examined the photocatalysis of glycerol using both pure TiO_2 and Pt/TiO_2, and has proposed several reaction pathways based on the intermediates formed. [43] Some of the intermediates that are present in the liquid state include acetol, acetaldehyde, methanol and ethanol, and the intermediates are present regardless of the photocatalyst. The benefit of the Pt co-catalyst, as discussed before, is to improve electron-hole pair separation, as well as to promote the rate-limiting half reaction of H_2 evolution.

$$2H^+ + 2e^- \rightarrow H_2$$

The variation of H_2 production with intensity of UV illumination was also investigated (Figure 2 (e), (f)). It was observed that the H_2 production rate had a linear relation with the intensity of light shone on the photocatalysts for the four temperatures tested. This shows that for light concentration up to the measured intensity do not affect the rate of H_2 production, and thus suggests the possibility of the use of solar concentrators to increase the temperature of the reactor.

Even though the performance of the photocatalysts are usually reported in mol/gh of hydrogen generation rate, it is dependent on various factors such as type and intensity of light source, illumination area, type of reactor. Using the apparent quantum yield (AQY) metric to determine the photocatalytic performance of the samples gives us a more consistent value as it factors into account the input power of the illumination source. This metric is defined as ratio of H_2 molecules generated to the incident power for a given wavelength of irradiation as follow: [11, 13]

$$AQY = \frac{Output\ of\ H_2\ per\ second}{Input\ Power} = \frac{No.of\ H_2\ generated\ per\ second\ \times 2}{No.of\ incident\ photons\ per\ second}$$

From the equation, the light to H_2 conversion efficiency was calculated to be 66.9% for the 3% CuO-loaded nanotubes sample at 90 °C at the highest intensity, which is much higher than the 10.3% efficiency calculated for the same sample at 25 °C. This suggests the considerable influences of temperature and co-catalyst-loading for remarkable increase in the photocatalysis efficiency.

Figure 2(g) and (h) shows the photocatalytic cyclic stability testing for nanoparticles and nanotubes samples as well as the 3% CuO-loaded counterparts, over a period of 4 hours of continuous testing under UV illumination for 4 cycles at 90 °C. From the figures seen, the initial H_2 evolution is approximately linear rate and tapered off towards the end of the 4 hours. It is postulated that the byproducts such as acetylaldehyde and acetic acid are formed from the sacrificial reagents during the photocatalysis process slowed down the rate of reaction.[44-47] The same trend was also seen for pure TiO_2 samples, albeit more obvious after a longer period of photocatalysis. However, the rate of H_2 evolution was restored once the photocatalysts were regenerated (details at the experimental section). Figure S4 show the initial H_2 evolution rate for each of the samples over the 4 cycles, and it can be seen that the

rates were fairly constant throughout the tests. The results were also consistent with those that were measured during the single run at 90 °C tests (Figure 2 (c),(d)).

Photocatalytic cyclic stability testing was also done under simulated solar irradiation, by means of a Xe lamp. Xe arc lamps have been widely used as an illumination source for solar simulators as even the unfiltered emission spectrum matches closely to that of natural sunlight. Also a Xe lamp would be able to provide consistent, reproducible measurements of photocatalytic activities which would be challenging under the natural sun where cloud cover and outdoor temperatures and activities would affect the measurements. Figure S5 shows the rates of H_2 evolution, as well as the total amount produced across the 4 cycles are consistent with each cycle, indicating stability of the photocatalysts under a broad spectrum illumination. The temperatures of the quartz reactors were also measured, and they were shown to stabilize at 42.0 °C – 43.0 °C after heating up from a temperature of 22.0 °C, in an ambient of 31.0 °C (± 1.0 °C).

Transient photovoltage measurement has been used routinely to find pseudo-first-order recombination rate constant which gives an indication of the carrier lifetimes. This small perturbation method used in photochemical electrochemical water splitting has shown that trap limited transport and recombination of electrons mechanisms correlate well with that for dye sensitized solar cells, as well as good agreement between the photovoltage and electron density measured with transient absorption spectroscopy.[48, 49] The pristine TiO_2 nanoparticles and nanotubes were measured under different temperatures to examine the effect of temperature on the electron lifetimes (Figure 3 (a), (b)). These exponential rise and decay is consistent with the exponential distribution of trap states below the TiO_2 conduction band, termed the multiple trapping model, while the time constant for the exponential decays gives the effective electron lifetimes.[49] Both samples consistently showed longer lifetimes of photogenerated electrons with increasing temperature at varying light intensities. This suggests that the higher temperature leads to an observed increased lifetime of the photogenerated carriers, hence suggesting that recombination rate is reduced, substantially improving H_2 generation rate as observed earlier.

Photocurrent measurements were carried out to investigate the effect of glycerol on the photocatalysts under different temperatures (Figure 3 (c)). A potential bias of 0.5V was set up between two electrically isolated regions of FTO with a continuous layer of TiO_2 residing on top to generate a photocurrent through the TiO_2 film. Almost no dark current was observed in

the deionized water without glycerol indicating that no dark reaction has occurred. When the light was switched on some photocurrent ~2.5 - 6.5 μA was observed, an indication of water splitting taking place. Glycerol was then added to the deionized water and the photocurrent was observed to increase to ~14 - 26 μA. Glycerol is a hole scavenger which serves to remove the photogenerated holes in the TiO_2 film.[11] This leads to a higher concentration of electrons remaining in the conduction band of TiO_2 resulting in a higher conductivity and photocurrent. The photocurrent increased with higher temperatures, which we postulate was due to the better hole scavenging effect of glycerol. This observation links back to the TPV results of a higher electron lifetime, as a lower rate of recombination would naturally infer a longer lifetime for the photogenerated electrons.

Simple prototypes for outdoor testing were constructed to demonstrate a proof-of-concept for broadband spectrum operation under natural sunlight, as well as the simplicity of this concept for practical photocatalysis applications. The first test was done with a parabolic reflector focusing sunlight onto a borosilicate round-bottomed flask, filled with 3% CuO-NT photocatalysts in glycerol-water solution (Figure 4 (a)). A slow initial H_2 evolution rate of 12.1 mmol/gh was observed after the first 10 min due to the gradual heating up of the water containing sacrificial agent from room temperature (22°C) (Figure 4 (b)). However, once the solution reached the maximum temperature of ~ 93 °C at 40 min, highest H_2 generation rate was recorded between the 40 to 50 min marks where the evolution rate reached 105 mmol/gh. The overall H_2 evolution measured for such simple photoreactor design was a high rate of ~ 65 mmol/gh. However, such simple reactor without insulation has the drawback of not retaining the temperature of the solution when the light irradiance fluctuates.

With this in mind, the second reactor was designed with the comparison done on the effect of insulation on the reactors. Two cylindrical quartz reactors were placed concurrently under the sun without any light concentration effect. One was placed in a box with insulation foam all around, leaving only a gap on top for light to shine through an acrylic window (Figure 4 (c)). The other was placed in the open, without any form of insulation. From Figure 4 (d), it is observed that the uninsulated quartz reactor performed better for the first two readings, as the uninsulated reactor heated up faster than the one in the insulation box. The reactor in the insulation box took 45 min to reach the temperature of 40 °C after which the H_2 generated from the insulated reactor began to exceed that of the uninsulated reactor. The maximum temperature attainable for the uninsulated reactor is higher than the insulated one as it reached to ~50 °C. As the photocatalytic reaction continued, it is apparent that the insulated

reactor steadily produced more H_2 than the uninsulated counterpart, due to heat absorption and retention through the black insulation foam. In general, the reactors have a higher temperature than ambient temperature of 31 °C due to the absorption of radiation through the solution and photocatalysts. The reactors had an initial H_2 evolution rate of ~1.22-1.26 mmol/gh within the first 20 min and subsequently reached 4.83 and 6.84 mmol/gh for the uninsulated and insulated reactors respectively. These outdoor testing clearly demonstrated that temperature has a crucial effect in increasing the rate of H_2 production, both from comparing the initial room temperature and elevated temperature rates, as well as comparing the insulated and uninsulated reactor rates.

CONCLUSION

This work demonstrates the utilization of the broadband solar spectrum to increase the H_2 evolution rate of a photocatalytic system, by converting the unused portion of solar spectrum to heat. Increasing the temperature of photocatalysis has shown to correlate to an increase in the electron lifetime in TPV measurements that is beneficial for photocatalysis reaction. Furthermore, the presence of CuO co-catalyst also reduces the electron-hole recombination by separating the photogenerated electron from the hole. CuO also contributed to a greater absorbance of the full spectrum of light and converted a portion of it to low grade heat. On the whole, a remarkable improvement in photocatalytic H_2 production up to 350-fold were measured for the pristine TiO_2 nanotubes with the double-effect of co-catalyst loading and operating at elevated photocatalysis temperature. An AQY of 66.9% was achieved under optimum CuO-loading at 90 °C, which is ~5-7 times improvement over most other earth abundant co-catalysts TiO_2 photocatalysts at room temperature. Finally, simple reactors were constructed to demonstrate the proof-of-concept harvesting of broadband solar energy for photon and heat conversions to enable practical and efficient solar-energy conversion photocatalysis.

EXPERIMENTAL

Synthesis of TiO_2 nanotubes -CuO composite

TiO_2 nanotube synthesis was adapted from an established hydrothermal synthesis process.[50] 1 g of P25 (Degussa) was added into 35 ml of 10 M NaOH and heated at 130 °C for 16 h in an

autoclave. The product was washed with 0.1 M HCl until the pH reached ~1 and subsequently rinse off to pH of 5-6. The suspension obtained was dried at 60 °C and then annealed at 450 °C for 2 h. CuO loading was done by wet impregnation.Different concentrations of $Cu(NO_3)_2$ (aq.) was mixed with TiO_2 nanotubes (NT) or P25 nanoparticles (NP). The mixture was then sonicated for 30 min and stirred for 2 h to ensure even mixing. Then the solution was dried at 60 °C and annealed at 350 °C for 5 h.

Materials characterizations

Scanning electron microscopy (SEM) optical characterizations were carried out using a JEOL FEG JSM 7001F operating at 15 kV. The structural properties were analyzed using transmission electron microscopy (TEM, Phillips FEG CM300) operating at 200 kV. X-ray diffraction (XRD, Philips X-ray diffractometer equipped with graphite-monochromated Cu Kα radiation at λ = 1.541 Å) measurements were used to identify the crystal structures. UV-visible absorption spectra were obtained using a Shimadzu UV-3600 UV-vis spectrophotometer. Specific surface areas were calculated by Brunauer–Emmett–Teller (BET) analysis conducted using Quantachrome Nova 1200 with N2 as the adsorbate at liquid nitrogen temperature.

Photocatalyst performance measurements

H_2 evolution measurements were conducted using 10 mg of photocatalysts in 10 ml of water with glycerol sacrificial reagent (20 % vol) in a 25 ml quartz reactor with a light emitting diode (LED) of 365 nm as illumination source. All LED intensities were measured with a Coherent PowerMax-USB PM3 sensor. The sealed quartz reactor was purged with Ar for 10 min. A water bath was used to control the temperature as required. H_2 gas concentration was measured by gas chromatogram (GC) (Shimadzu, GC 2014AT). For heat absorbance test, the same quartz reactors were used with the same amount of photocatalysts (NT and CuO-NT) and electrolyte. The reactors were purged with Ar and photocatalysts were exposed to UV to allow the reduction of CuO-NT. The quartz reactors were then immersed in an ice water bath for 30 min, and the temperature of the reagents in the quartz reactors were measured to be 0 °C (± 0.2 °C) upon starting the test by using a thermometer inserted into the reactor. The quartz reactors were placed in front of a 300W Xe lamp with an intensity of 1000W/m² (Perkin Elmer, PE300BFA). The ambient temperature was kept constant at 28.0 °C (± 0.2 °C), and the temperature of the reagents were measured every 30 s for 30 min. For cyclic stability test done using UV LED, 10 mg of photocatalysts were used for photocatalytic reaction for 4 h in a 90.0 °C (±1.0 °C) water bath. They were then centrifuged down, washed with

deionized water and dried overnight at 120 °C. The dried powders were exposed to UV light (Novascan UV surface decontamination system) for 5 min to remove any organic residue. The photocatalysts were then used for the stability test for 4 consecutive hours for 4 cycles, with the same washing procedure stated above. Similarly for cyclic stability test done under simulated solar irradiation, the quartz reactors with CuO-NP or CuO-NT were placed in front of a 300W Xe lamp with an intensity of 1000 W/m^2. The reactors were allowed to heat up naturally in air without the use of a water bath. The washing procedure in between cycles is the same as above.

Outdoor measurements were done on 16 Feb 2015, 12 to 1pm, maximum solar intensity 950 W/m^2, ambient temperature 33 °C with a parabolic concentrator (30 cm diameter) onto a borosilicate round bottom flask containing 25 mg of 3% CuO-NT photocatalyst in 50 ml of water with glycerol (20 % vol) (Figure 4a). Another outdoor measurements with solar insulation were done on 13 Jan 2015, 1 to 3 pm, maximum solar intensity 1020 W/m^2, ambient temperature 31 °C concurrently using 2 separate quartz reactors. One was placed in a insulation box surrounded by ArmorFlex insulation (Figure 4c) with an acrylic window (3mm thick) while the other reactor was placed in the open without insulation. Both reactors contain 10 mg of 3% CuO-NT photocatalyst in 10 ml of water with glycerol (20 % vol). Both quartz reactors were placed perpendicular to the sun's rays, and the positions were adjusted every 15 mins. Similarly, all reactors are purged before H_2 measurements were measured with the GC at regular intervals.

Transient photovoltage (TPV) measurements

Slurries were prepared by mixing 1 g TiO_2 powders in 10 g of α-Terpineol and 0.5 g of ethyl cellulose dissolved in ethanol. TPV samples were prepared by spin coating the slurry on fluorine doped tin oxide (FTO) substrates of the size 3 x 5 cm^2 (QZ hybrid supplies, <10 Ω per sq) and annealed at 450 °C for 2 h. The transient photovoltage measurements were taken using the Parstat 4000, with a 2 electrode configuration using the photoanode prepared on FTO and a Pt foil counter electrode immersed in a solution of 0.1M Na_2SO_4 with 20 % vol glycerol. The electrolyte was purged with Ar to remove any dissolved gas in before the experiments and in between measurements. The illumination source, LED (365 nm) connected to a function generator (Agilent 35522B) generating a square wave at 5 different amplitudes (from 100-300 mV) for various light intensities. The whole cell was placed on a hotplate stirrer to maintain the temperature and the ionic transport of the products. Signals

were filtered for 50 Hz noise and the photovoltage rise and decay time constants were determined by fitting single exponentials.

Photocurrent measurements

A TiO_2 film was prepared using the NT slurry onto FTO substrate similar to the above. Part of the FTO was removed through the centre so that the substrate has 2 isolated conducting regions, prior to spin coating. The prepared sample was then immersed into deionized water purged with argon and photocurrent was measured using a 2 electrode configuration with a 0.5V potential between them. The LED was then switched on at the 60 s mark, and 1.0ml of a 10% vol glycerol solution added at the 120 s mark. The LED was switched off after another 60 s. This was done at 4 different temperatures.

ACKNOWLEDGEMENT

This work is supported by the MOE R-263-000-B38-112 and R-263-000-B63-112.

References

1. A. Wold, *Chem. Mater.*, 1993, **5**, 280-283.
2. A. L. Linsebigler, G. Lu and J. T. Yates, *Chem. Rev.*, 1995, **95**, 735-758.
3. X. Chen and S. S. Mao, *Chem. Rev.*, 2007, **107**, 2891-2959.
4. M. Ni, M. K. H. Leung, D. Y. C. Leung and K. Sumathy, *Renew. Sustainable Energy Rev.*, 2007, **11**, 401-425.
5. A. Kudo and Y. Miseki, *Chem. Soc. Rev.*, 2009, **38**, 253-278.
6. M. Kitano, M. Takeuchi, M. Matsuoka, J. M. Thomas and M. Anpo, *Catal. Today.*, 2007, **120**, 133-138.
7. K. Maeda and K. Domen, *J. Phys. Chem. C*, 2007, **111**, 7851-7861.
8. M. Hara, T. Kondo, M. Komoda, S. Ikeda, J. N. Kondo, K. Domen, K. Shinohara and A. Tanaka, *Chem. Commun.*, 1998, DOI: 10.1039/A707440I, 357-358.
9. J. Bandara, C. P. K. Udawatta and C. S. K. Rajapakse, *Photochemical & Photobiological Sciences*, 2005, **4**, 857-861.
10. H.-J. Choi and M. Kang, *Int. J. Hydrogen Energy*, 2007, **32**, 3841-3848.
11. J. Yu, Y. Hai and M. Jaroniec, *J. Colloid Interface Sci.*, 2011, **357**, 223-228.
12. S. Xu and D. D. Sun, *Int. J. Hydrogen Energy*, 2009, **34**, 6096-6104.
13. Z. Jin, X. Zhang, Y. Li, S. Li and G. Lu, *Catal. Commun.*, 2007, **8**, 1267-1273.
14. W. Wang, S. Liu, L. Nie, B. Cheng and J. Yu, *Phys. Chem. Chem. Phys.*, 2013, **15**, 12033-12039.
15. D. Kondarides, V. Daskalaki, A. Patsoura and X. Verykios, *Catal Lett*, 2008, **122**, 26-32.
16. Y. Wang, J. Yu, W. Xiao and Q. Li, *J. Mater. Chem. A*, 2014, **2**, 3847-3855.
17. M. N. Chong, B. Jin, C. W. K. Chow and C. Saint, *Water Research*, 2010, **44**, 2997-3027.
18. S. Hoang, S. Guo, N. T. Hahn, A. J. Bard and C. B. Mullins, *Nano Lett.*, 2012, **12**, 26-32.
19. X. Tong, P. Yang, Y. Wang, Y. Qin and X. Guo, *Nanoscale*, 2014, **6**, 6692-6700.
20. Y. Gai, J. Li, S.-S. Li, J.-B. Xia and S.-H. Wei, *Phys. Rev. Lett.*, 2009, **102**, 036402.
21. X. Ma, Y. Wu, Y. Lu, J. Xu, Y. Wang and Y. Zhu, *J. Phys. Chem. C*, 2011, **115**, 16963-16969.
22. V. M. Aroutiounian, V. M. Arakelyan and G. E. Shahnazaryan, *Sol. Energy*, 2005, **78**, 581-592.
23. X. Chen, L. Liu, P. Y. Yu and S. S. Mao, *Science*, 2011, **331**, 746-750.
24. R. M. Navarro Yerga, M. C. Álvarez Galván, F. del Valle, J. A. Villoria de la Mano and J. L. G. Fierro, *ChemSusChem*, 2009, **2**, 471-485.
25. R. Williams, *The Journal of Chemical Physics*, 1960, **32**, 1505-1514.
26. A. B. Ellis, S. W. Kaiser, J. M. Bolts and M. S. Wrighton, *J. Am. Chem. Soc.*, 1977, **99**, 2839-2848.
27. Z. Hu and J. C. Yu, *J. Mater. Chem. A*, 2013, **1**, 12221-12228.
28. J. Zhang, Q. Xu, S. Z. Qiao and J. Yu, *ChemSusChem*, 2013, **6**, 2009-2015.
29. W. Xitao, L. Rong and W. Kang, *J. Mater. Chem. A*, 2014, **2**, 8304-8313.
30. M. G. Walter, E. L. Warren, J. R. McKone, S. W. Boettcher, Q. Mi, E. A. Santori and N. S. Lewis, *Chem. Rev.*, 2010, **110**, 6446-6473.
31. F. Auzel, *Chem. Rev.*, 2004, **104**, 139-174.
32. M. Haase and H. Schäfer, *Angew. Chem. Int. Ed.*, 2011, **50**, 5808-5829.
33. X. Jiang, Y. Zhang, J. Jiang, Y. Rong, Y. Wang, Y. Wu and C. Pan, *J. Phys. Chem. C*, 2012, **116**, 22619-22624.
34. Y. H. Hu, *Angew. Chem. Int. Ed.*, 2012, **51**, 12410-12412.
35. X. Pan, M.-Q. Yang, X. Fu, N. Zhang and Y.-J. Xu, *Nanoscale*, 2013, **5**, 3601-3614.
36. Q. Kang, J. Cao, Y. Zhang, L. Liu, H. Xu and J. Ye, *J. Mater. Chem. A*, 2013, **1**, 5766-5774.
37. K. Lalitha, G. Sadanandam, V. D. Kumari, M. Subrahmanyam, B. Sreedhar and N. Y. Hebalkar, *J. Phys. Chem. C*, 2010, **114**, 22181-22189.
38. G. Li, N. M. Dimitrijevic, L. Chen, T. Rajh and K. A. Gray, *J. Phys. Chem. C*, 2008, **112**, 19040-19044.
39. N.-L. Wu and M.-S. Lee, *Int. J. Hydrogen Energy*, 2004, **29**, 1601-1605.

40. T. Ito, Y. Nakashimada, K. Senba, T. Matsui and N. Nishio, *J. Biosci. Bioeng.*, 2005, **100**, 260-265.
41. S. Papanikolaou and G. Aggelis, *Lipid Technology*, 2009, **21**, 83-87.
42. R. Ruhal, S. Aggarwal and B. Choudhury, *Green Chemistry*, 2011, **13**, 3492-3498.
43. P. Panagiotopoulou, E. E. Karamerou and D. I. Kondarides, *Catal. Today.*, 2013, **209**, 91-98.
44. V. Gombac, L. Sordelli, T. Montini, J. J. Delgado, A. Adamski, G. Adami, M. Cargnello, S. Bernal and P. Fornasiero, *J. Phys. Chem. A*, 2010, **114**, 3916-3925.
45. U. Diebold, *Surf. Sci. Rep.*, 2003, **48**, 53-229.
46. S. Klosek and D. Raftery, *J. Phys. Chem. B*, 2001, **105**, 2815-2819.
47. S. Pilkenton, S.-J. Hwang and D. Raftery, *J. Phys. Chem. B*, 1999, **103**, 11152-11160.
48. A. J. Cowan, W. Leng, P. R. F. Barnes, D. R. Klug and J. R. Durrant, *Phys. Chem. Chem. Phys.*, 2013, **15**, 8772-8778.
49. W. H. Leng, P. R. F. Barnes, M. Juozapavicius, B. C. O'Regan and J. R. Durrant, *J. Phys. Chem. Lett.*, 2010, **1**, 967-972.
50. T. Kasuga, M. Hiramatsu, A. Hoson, T. Sekino and K. Niihara, *Langmuir*, 1998, **14**, 3160-3163.

Figure captions:

Figure 1 (a) SEM and (b) TEM of TiO_2 nanotubes loaded with CuO nanoparticles. (b, inset) HRTEM of a CuO nanoparticle with corresponding (111) plane of CuO. (c) XRD pattern of CuO loaded NP and NT. (d) UV-Vis absorption spectra of nanoparticles and nanotubes, with and without CuO nanoparticles, (top) before and (below) after UV illumination (e) Nitrogen adsorption/desorption isotherm of nanotubes with (inset) BJH pore size distribution.

Figure 2 Top row, NP photocatalysts: (a) H_2 evolution rate with different wt. % CuO loading at room temperature. (c) H_2 evolution rate with and without CuO loading at different temperatures. (e) H_2 evolution rate at different light intensities. (g) Amount of H_2 evolved for cyclic stability test under UV LED irradiation at 90 °C, measured for 4 cycles.
Bottom row, NT photocatalysts: (b, d, f, h) Same as top row.

Figure 3 TPV measurements of (a) NP and (b) NT at varying temperatures; and (c) photocurrent measurements of NT film showing effect of glycerol at different temperatures.

Figure 4 (a) H_2 evolution under solar irradiation with a 30 cm diameter concentrator and (b)corresponding H_2 production (solid marker) and temperature (open marker), ; (c) model of quartz reactor in insulation foam for direct solar irradiation (no concentrator); (d) corresponding H_2 production (solid marker) and temperature (open marker), with and without insulation .

Figure 1

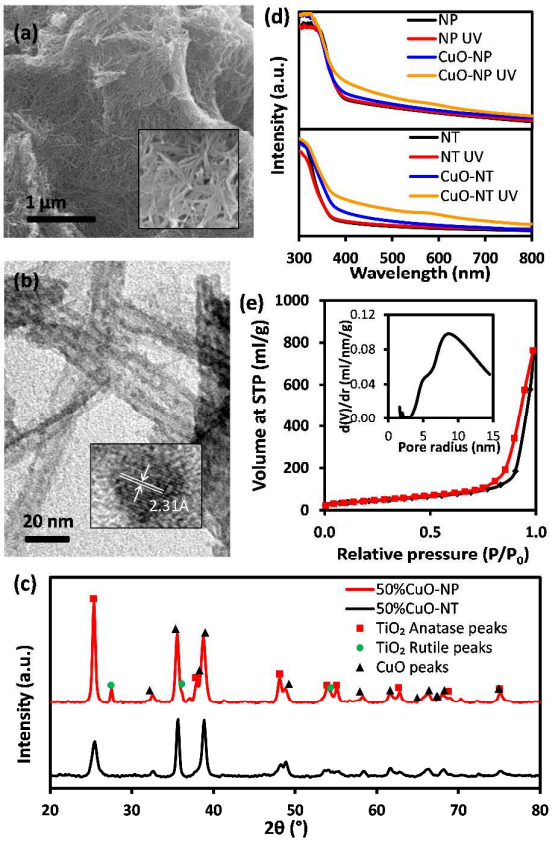

Figure 2

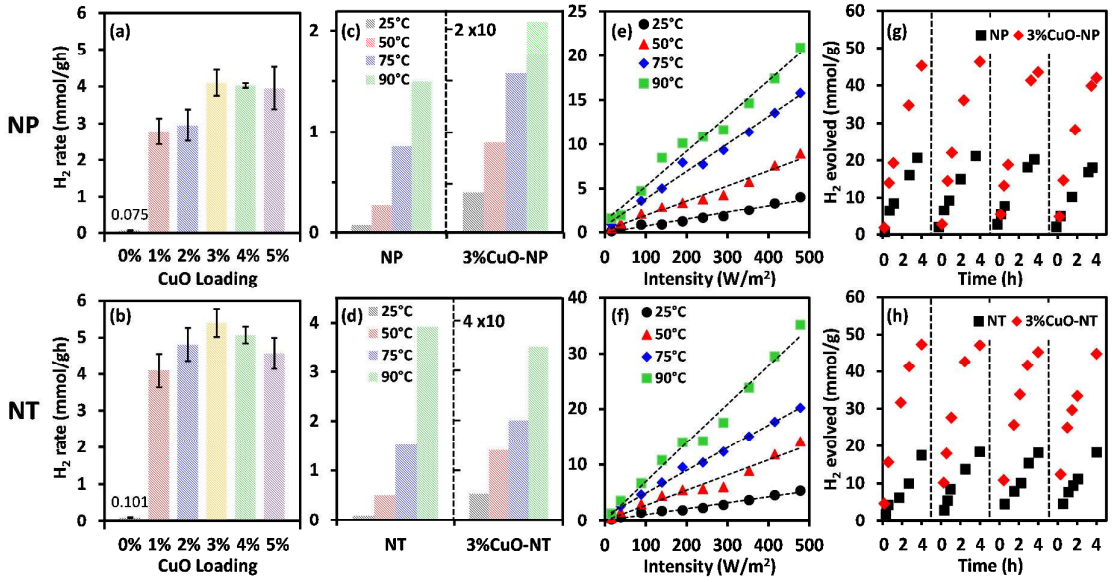

Figure 3

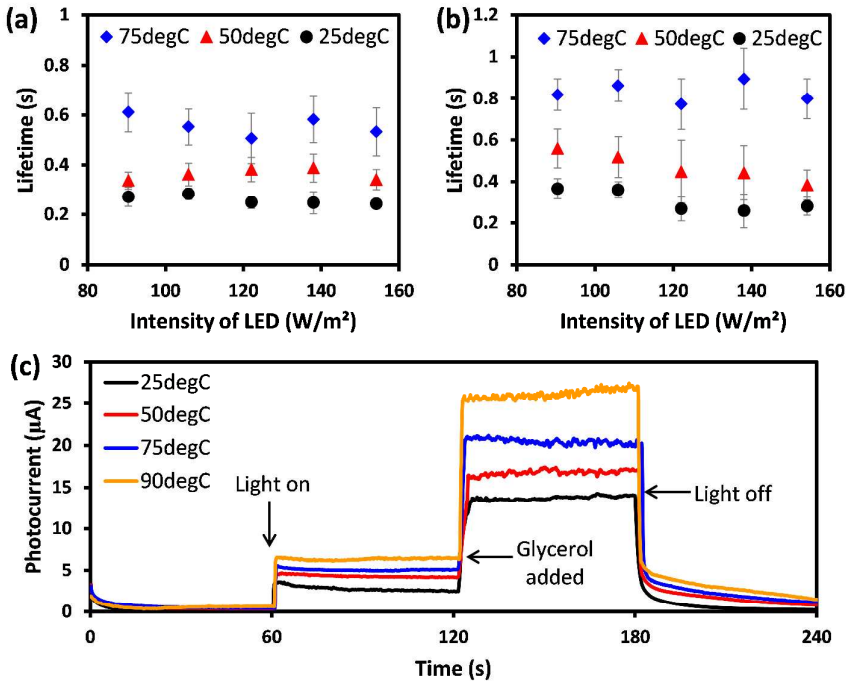

Figure 4

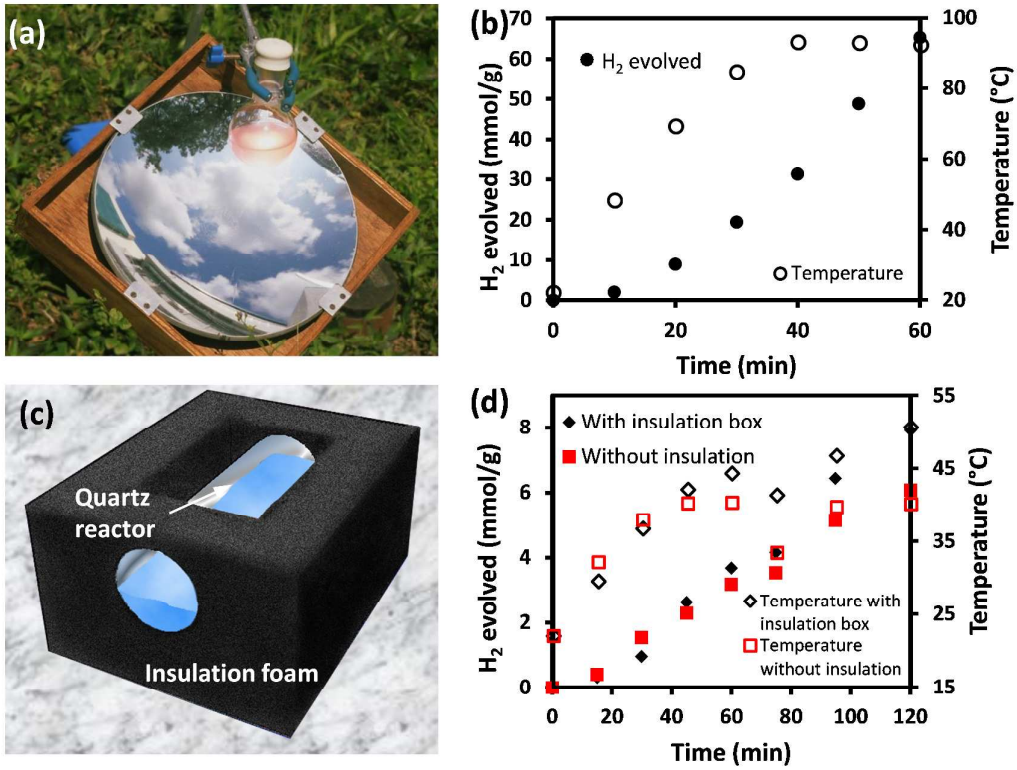

Graphical Abstract Entry

Broadband solar spectrum harvested as heat increased H_2 generation from pure TiO_2 nanoparticles by 40-fold, and when coupled with CuO nanoparticles gave an apparent quantum yield of 66.9% at 365nm.